Halving warming with idealized solar geoengineering moderates key climate hazards

Peter Irvine[1]*, Kerry Emanuel[2], Jie He[3,4,5], Larry W. Horowitz[4], Gabriel Vecchi[6], David Keith[1]

* Contact: Peter_irvine@fas.harvard.edu

1 – John A. Paulson School of Engineering and Applied Sciences, Harvard University, Cambridge, MA, USA

2 – Lorenz Center, Massachusetts Institute of Technology, MA, USA

3 - The Program in Atmospheric and Oceanic Sciences, Princeton University, NJ, USA

4 – National Oceanic and Atmospheric Administration, Geophysical Fluid Dynamics Laboratory, Princeton, NJ, USA

5 - School of Earth and Atmospheric Sciences, Georgia Institute of Technology, GA, USA

6 - Department of Geosciences and the Princeton Environmental Institute, Princeton University, NJ, USA

Solar geoengineering (SG) could restore average surface temperatures by increasing the planetary albedo [1–4], but doing so would reduce precipitation [5–7]. Solar geoengineering might, thus, increase climate risks for some regions, even as it reduced globally-aggregated risks[8–10]. We analyse the fraction of locations that see local climate change exacerbated or moderated by SG. Rather than restoring temperatures, we assume that SG is applied to halve the warming produced by doubling CO_2 (half-SG). We use HiFLOR, a 25 km resolution tropical-cyclones-permitting model with a substantially improved representation of present-day precipitation extremes[11], and a dozen models from the Geoengineering Model Intercomparison Project (GeoMIP)[12]. In HiFLOR, half-SG offsets most of the CO_2-induced increase of simulated tropical cyclone intensity, while it does not exacerbate the effect of doubling CO_2 on water availability or extreme precipitation averaged over any IPCC-SREX region; and, less than 0.4% of the land surface sees exacerbation of extreme precipitation or water availability. Concerns about the inequality of the impacts of solar geoengineering are appropriate, yet the quantitative extent of inequality may be overstated[13]. Our results suggest that no region would see aggregate impacts of climate change exacerbated by solar geoengineering that halves global temperature change.

The idea that an engineered increase in planetary albedo might offset greenhouse gas (GHG)-driven warming is more than half a century old [1]. Early studies addressed the technology and its policy implications [2–4], yet it was not until 2000 that a climate model was first used to study the spatial pattern of climate response to Solar Geoengineering (SG) [7]. Since then, at least 100 papers, including many from GeoMIP, have addressed the climate response to various SG scenarios [12,14]. Some methods of SG could enable the world to keep global mean temperatures below the 1.5°C warming threshold [15–17]. But, global temperature targets are proxies for local changes in climate variables that drive impacts. SG might hypothetically reduce global mean surface temperature while still making most people worse off. Indeed, concerns about the climate's response to SG have focused on regional disparities in climate impacts and reductions in precipitation in particular [13,18].

The policy-relevance of prior analysis of the climate response to SG has been limited by several choices. First, many studies focused only on 2-m air temperature (T) and precipitation (P); yet without accounting for evaporation (E), precipitation alone is not an effective proxy for water

availability or agricultural productivity[19]. Second, many studies assumed SG was used to substitute for emission cuts by offsetting all GHG-induced warming, substantially reducing the strength of the hydrological cycle [6,7,12], and few existing studies evaluated scenarios where SG complements emissions reductions without offsetting all warming [16,20]. Third, despite concern about the potential for SG to worsen climate impacts in some regions, no prior analysis has estimated the fraction of locations that see local climate change exacerbated by SG, where "exacerbated" means that the absolute deviation from control is increased by SG.

We analyse the distribution of climate changes resulting from reducing the solar constant to offset roughly half the radiative forcing from doubling CO_2. A spatially uniform reflective stratospheric aerosol layer, which could be achieved by adjusting aerosol injection using feedback [21,22], would produce a similar radiative forcing to a solar constant reduction. Even with a uniform distribution, stratospheric sulphate SG will differ from a solar constant reduction in that sulphates heat the lower stratosphere, perturb the ozone layer, and increase the ratio of diffuse to direct light [15]. Each of these effects can be reduced by choices of alternate non-sulphate aerosol, though their side-effects are less well understood because there is no direct natural analogue [23]. We nevertheless choose solar constant reduction as a benchmark because, given the diverse implementations of aerosols in models, solar modification allows more direct tests of inter-model differences in climate response to SG.

We use the GFDL HiFLOR model run at a horizontal resolution of ~25 km (see Methods)[11,24,25]. The model endogenously generates tropical cyclones with up to Category 5 intensity and significantly reduces biases in regional temperature and precipitation extremes of the current climate compared to lower resolution versions of its model family [11,24]. Relative to a present-day control experiment, we compare the climate response over a 100-year period of an experiment in which CO_2 is doubled ($2xCO_2$ experiment) to that of an experiment in which the solar constant is reduced by 1% to approximately offset half of the warming from the CO_2 doubling (half-SG experiment, see Methods). We test the robustness of the HiFLOR results by comparing them to those of 12 climate models that participated in the GeoMIP G1 experiment [12,26], in which the global mean temperature response to an instantaneous quadrupling of CO_2 concentrations is fully offset using a model-dependent reduction in solar constant of roughly 4%. We generate a synthetic half-SG scenario for each of the GeoMIP models by linearly scaling all variables to a value midway between their G1 and $4xCO_2$ values (see Methods).

We analysed annual means of T, P - E (PE), yearly maximum temperature (Tx), yearly maximum precipitation in a 5-day window (Px), and the power dissipation index (PDI) of tropical cyclones (see Methods) [27]. These five variables span most of the drivers of the "key risks of climate change" identified by the IPCC with the notable exception of sea-level rise (Extended Data Table 1). In contrast to much of the prior literature on solar geoengineering, we exclude annual-mean P as it is a less effective proxy for water availability than PE [19], and a less effective proxy for flood risk than Px[28] (though results are included in Extended Data).

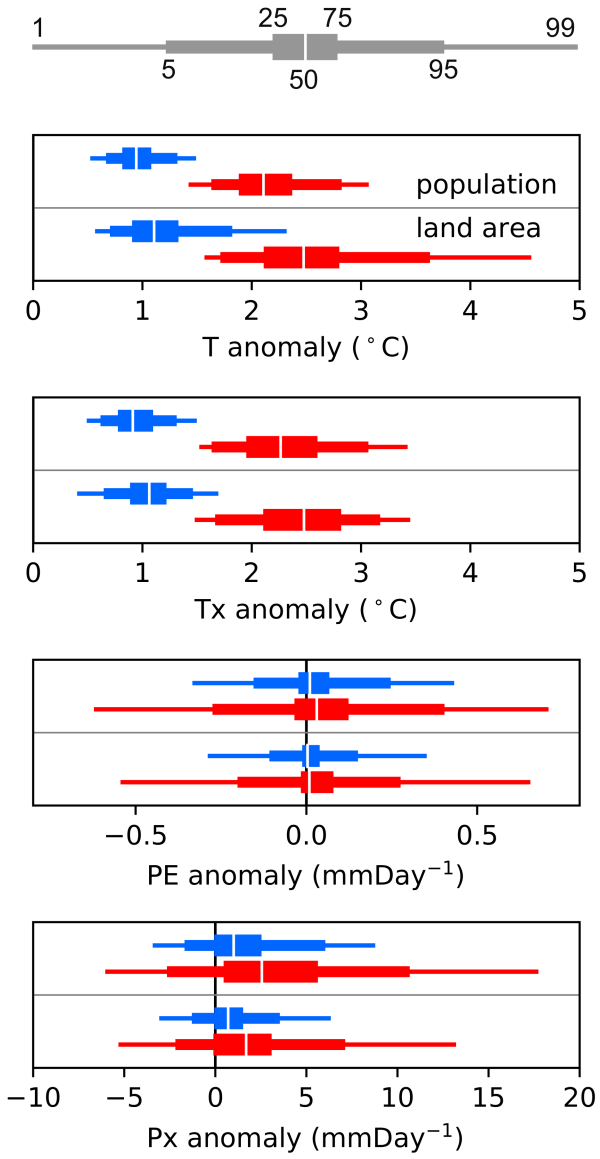

Figure 1. The distribution of 2xCO_2 and half-SG anomalies by land area and population. The distribution of 2xCO_2 (red) and half-SG (blue) anomalies versus control for the HiFLOR model are plotted by land area (bottom), excluding Greenland and Antarctica, and by population (top) for, from top to bottom, surface air temperature (T), maximum annual T (Tx), precipitation – evaporation (PE), maximum annual 5-day precipitation (Px) (see Methods). The legend above illustrates how the percentiles of the distribution are shown.

Figure 1 shows the distribution of climate changes under *2×CO_2* and *half-SG* versus the control. Since we are focusing on changes relevant to human and terrestrial ecological impacts, we examine land only, excluding Greenland and Antarctica, and compare area-weighted and population-weighed results. It is well known that SG suppresses the hydrological cycle and previous work suggested SG causes drying [5,18,26]. The *half-SG* scenario reduces the global average *P* increase from 3.0 % under *2xCO_2* to 0.5% under *half-SG*. Perhaps surprisingly, *half-SG* also reduces the fraction of land surface that sees drying as measured by a decrease in PE. Under *2×CO_2*, 3.7% of land surface sees a reduction of PE by more than 0.25 mm day^{-1}, whereas only 1.4% see the same drying under *half-SG*. The substantial reduction in the magnitude of both positive and negative anomalies shown in Figure

1 holds for the synthetic half-SG GeoMIP results, for percentage change and standard deviation normalized anomalies, and for precipitation (Extended Data Figures 1-3).

	Fraction Exacerbated				Fraction Moderated			
	HiFLOR	GeoMIP			HiFLOR	GeoMIP		
		Med	Min	Max		Med	Min	Max
T	0.0 %	0.0 %	0.0 %	0.0 %	100.0 %	100.0 %	99.2 %	100.0 %
Tx	0.0 %	0.0 %	0.0 %	0.3 %	100.0 %	100.0 %	98.9 %	100.0 %
PE	0.4 %	1.9 %	0.3 %	4.8 %	26.4 %	29.6 %	22.3 %	65.9 %
Px	0.4 %	0.8 %	0.1 %	7.3 %	41.6 %	44.9 %	28.2 %	60.9 %

Table 1. The fraction of the land surface that sees the effects of 2xCO_2 (relative to control) significantly exacerbated or moderated by half-SG. The percentage of the land area (excluding Greenland and Antarctica) experiencing a statistically significantly greater (exacerbated) or lesser (moderated) absolute magnitude of anomaly for half-SG compared to 2xCO2 (see Methods). Median, minimum and maximum for GeoMIP are calculated across the ensemble of individual model results.

Which regions are made worse off? Half-SG reduces the fraction of land area experiencing extreme climatic changes (Figure 1), but that does not tell us what fraction of points see their climate made worse. To test this, we define the effects of climate change as exacerbated if the absolute magnitude of the half-SG anomaly from the control is significantly greater than the 2×CO_2 anomaly, and that they are moderated if half-SG significantly reduces the absolute magnitude of the anomaly. If the control climate is assumed to be preferable to a disturbed climate, then exacerbated/moderated implies that the region is worse/better off. But, this will not always be true as some communities may prefer the altered climate. Table 1 shows the fraction of the land surface where half-SG exacerbates or moderates the effects of 2xCO_2 computed using a set of 90% *t*-tests applied to the values at each grid-point (see Methods). T and Tx changes are moderated over almost the entire land surface across all models. For PE and Px, the area moderated is far greater than the area exacerbated in the HiFLOR model and the GeoMIP ensemble. But note that many points do not show a significant change (do not pass the *t*-test). Results are similar when weighted by population and if calculated on a seasonal basis, though the fraction exacerbated in HiFLOR is somewhat greater for PE and Px at ~1 % (Extended Data Tables 2 and 3).

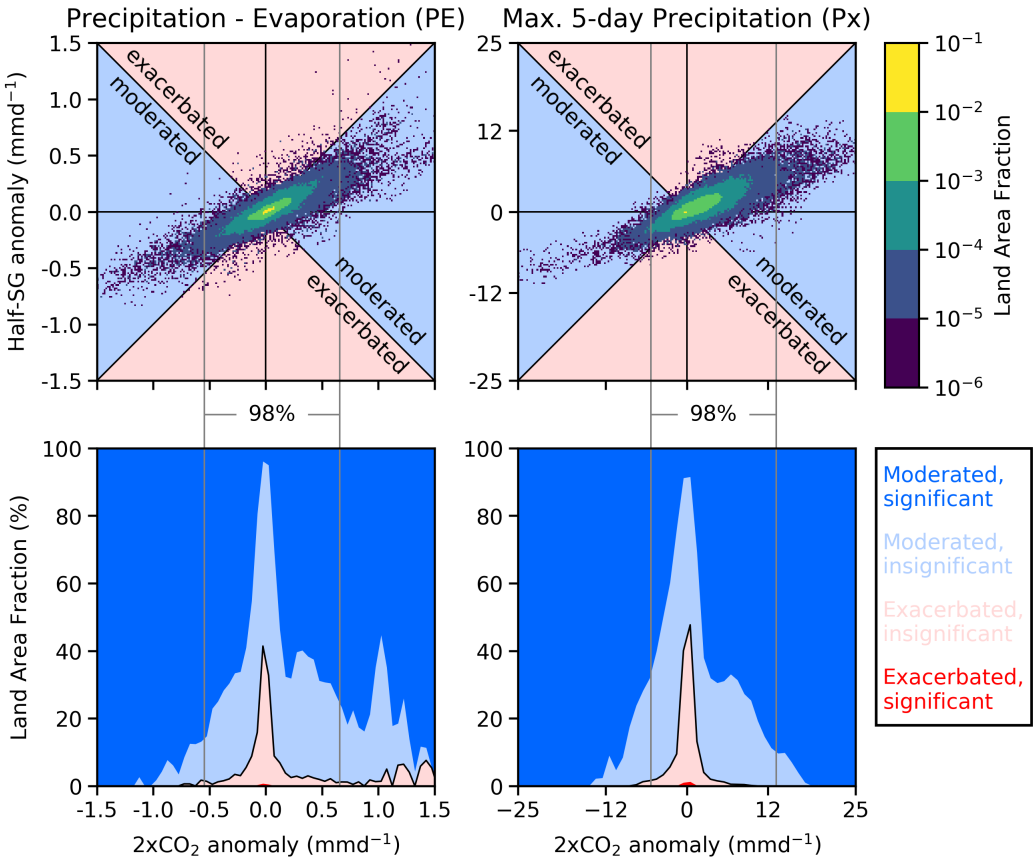

Figure 2. The joint distribution of 2xCO$_2$ and half-SG anomalies with results for the fraction of the land surface where half-SG exacerbates or moderates the climate trend. Top, 2D-histograms show the distribution across the land area, excluding Greenland and Antarctica, of the 2xCO$_2$ and half-SG anomalies versus control in precipitation minus evaporation (PE, left) and maximum 5-day precipitation (Px, right). To generate the bins for the 2D-histogram, the X and Y axes are divided into 200 intervals. The fraction of the land area with anomalies that fall into each bin are indicated by the colour scale, empty bins are not plotted. All points falling closer to the x-axis than the diagonal 1:1 lines see the magnitude of the trend reduced (moderated, blue backround) by half-SG and all those above and below these lines see the magnitude of the trend increased (exacerbated, pink background). Note all points, including those that don't see significant change are plotted. Bottom, the fraction of the area in which the impacts of 2xCO$_2$ are exacerbated (red) or moderated (blue) by half-SG as a function of the 2xCO$_2$ anomaly. Bold colours indicate statistically significant results and pale colours indicate insignificant results.

Figure 2 compares 2xCO$_2$ and half-SG anomalies (relative to control) of all land points and shows the fraction of points that are exacerbated or moderated as a function of the 2×CO$_2$ anomaly. Since points with no change under 2xCO$_2$ cannot see that change reduced, the fraction moderated tends to zero as the 2xCO$_2$ anomaly tends to zero. Points with large anomalies under 2xCO$_2$ are almost all moderated, while the points that are exacerbated almost all experience very small climatic change, i.e., those regions experiencing the greatest climate change are most likely to see it reduced by half-

SG. Similar results are found for precipitation, while temperature is significantly reduced at all locations (Extended Data Fig 4).

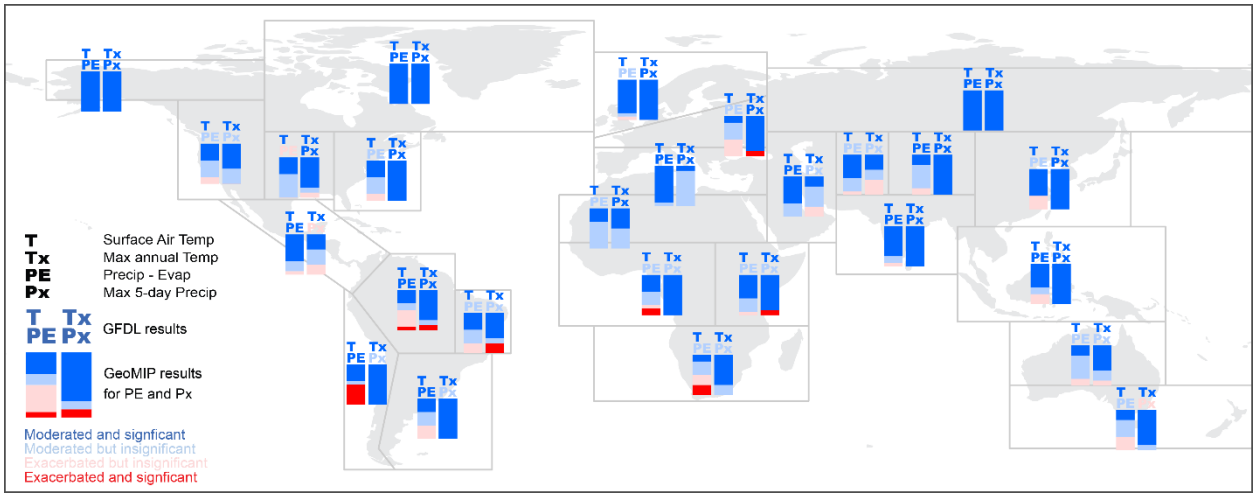

Figure 3. Regional distribution of where half-SG moderates or exacerbates the absolute magnitude of 2xCO_2 anomalies in HiFLOR (for T, Tx, PE, and Px) and the GeoMIP ensemble (PE and Px). Regions where half-SG moderates (blue) or exacerbates (red) the absolute magnitude of the 2xCO_2 climate anomalies relative to control are illustrated. Statistically significant results are indicated with bold colours whereas insignificant results are shown with pale colours (see Methods). The results for the GeoMIP models are shown for PE (left-column) and Px (right-column) with the columns coloured to indicate the fraction of GeoMIP models with each result. All GeoMIP models show a statistically significant reduction in T and Tx in all regions (not shown). Note, all model-regions which show a statistically significantly greater change for half-SG see greater PE in half-SG than in 2xCO_2 or the control, and less Px in half-SG than in 2xCO_2 or the control.

Only the strongest climate trends are detectable at small spatial scales; to test for weaker, larger-scale trends we aggregate results to the representative climate regions used in the IPCC Special Report on Extremes (SREX, see Methods). Figure 3 provides a global overview of the effects of SG on the climate variables assessed here, allowing a qualitative evaluation of whether a region would expect to see aggregate climate risks moderated or exacerbated under half-SG compared to 2xCO_2. None of the four variables are exacerbated (under a 90% *t*-test) by half-SG in the HiFLOR model in any region. A few regions show PE or Px exacerbated in at least one GeoMIP model, though in only Western South America and South Africa for PE do the number of models showing an exacerbation exceed the number showing a moderation.

Note, however that in the model regions where half-SG exacerbates change, all had a larger PE in half-SG than either 2xCO_2 or control. So, in the few regions where half-SG exacerbates climate change, it increases water availability. This stands in contrast to previous studies and commentary which highlighted concerns that SG would lead to drought [6,10,18]. For Px, in all model regions where half-SG exacerbates change, there is less extreme precipitation than in either 2xCO_2 or control, indicating less risk of flooding.

Finally, we examined the global intensity of tropical cyclones, including hurricanes and typhoons; directly simulating tropical cyclone response to solar geoengineering in a global model for the first time [29,30]. 2xCO_2 increases the sum of the power dissipation index over all tropical cyclones in HiFLOR by 17.6% compared to the control. Half-SG offsets most of this, reducing the increase in PDI to 2.4%.

As there is presently substantial uncertainty in regional projections of TC activity changes [31,32], in this paper we provide only the global results. In addition, we downscaled the HiFLOR output using the technique of Emanuel et al. (2008)[31] to produce 40,000 synthetic cyclones globally in years 100-300 of the control and 2xCO_2 climates, and 26,000 events in years 171-300 of the half-SG climate (see Methods). The downscaled storms show a much weaker response than HiFLOR, with a 5.1% increase in PDI in 2xCO_2 and a 2.0% decrease in half-SG, both relative to the control. This result differs substantially from downscaling CMIP5 models for emissions pathway RCP 8.5[33], which showed large increases in power dissipation. We speculate that well-resolved tropical cyclones in the fully coupled HiFLOR model may retard changes in monthly mean potential intensity[34], damping the response of synthetic storms to climate change.

We focused on an idealized SG scenario that approximately halves the warming from doubling CO_2, and so more-or-less restores the intensity of the hydrological cycle, rather than the typical scenario in which SG offsets all warming. Extended Data Figure 5 shows how the outcomes change as a function of the level of solar constant reduction and makes clear that beyond offsetting around half of the warming from 2xCO_2, the marginal benefits of further cooling decline and the fraction of the land in which climate change is exacerbated grows. While we do not claim that halving warming is necessarily optimal, we suggest it is a better starting point for analysis than a complete offset scenario, as it avoids more-than-reversing many climate trends as happens under scenarios which offset all warming.

It would be premature to conclude from this study that no region would experience greater aggregate climate risks in a real-world deployment of SG that halved anthropogenic warming, as we analysed an idealized scenario and a limited set of climate variables. Our results do not, however, support the common claims that SG would inevitably lead to significant harms to some regions[18], nor the claims that SG's benefits and harms always have a strongly unequal distribution[13].

Acknowledgements

We acknowledge the World Climate Research Programme's Working Group on Coupled Modelling, which is responsible for CMIP, and we thank the climate modeling groups for producing and making available their model output. For CMIP the U.S. Department of Energy's Program for Climate Model Diagnosis and Intercomparison provides coordinating support and led development of software infrastructure in partnership with the Global Organization for Earth System Science Portals. We thank all participants of the Geoengineering Model Intercomparison Project and their model development teams, CLIVAR/WCRP Working Group on Coupled Modeling for endorsing GeoMIP, and the scientists managing the Earth System Grid data nodes who have assisted with making GeoMIP output available. The authors acknowledge the help of Charles Curry who provided the extreme indices data for the GeoMIP ensemble. The authors acknowledge Robert Stanhope for help finalizing the figures. The authors would like to thank David Fahey and Ken Caldeira for comments on the draft and Lee Miller, Gernot Wagner and Daniel Kluger for helpful discussions on the statistical approach.

References

1. PSAC *et al. Restoring the quality of our environment*. (President's Science Advisory Committee, 1965).
2. Keith, D. W. & Dowlatabadi, H. A serious look at geoengineering. *Eos* **73**, 289–292 (1992).
3. Schelling, T. C. Climatic Change: Implications for Welfare and Policy. in *Changing Climate* (eds. Nierenberg, W. A. et al.) (National Academy of Sciences, 1983).
4. Teller, E., Wood, L. & Hyde, R. Global warming and ice ages: I. Prospects for physics-based modulation of global change. (1997).
5. Tilmes, S. *et al.* The hydrological impact of geoengineering in the Geoengineering Model Intercomparison Project (GeoMIP). *J. Geophys. Res. Atmospheres* **118**, 11036–11058 (2013).
6. Lunt, D. J., Ridgwell, A., Valdes, P. J. & Seale, A. 'Sunshade World': A fully coupled GCM evaluation of the climatic impacts of geoengineering. *Geophys. Res. Lett.* **35**, L12710 (2008).
7. Govindasamy, B. & Caldeira, K. Geoengineering Earth's radiation balance to mitigate CO2-induced climate change. *Geophys. Res. Lett.* **27**, 2141–2144 (2000).
8. Irvine, P. J., Ridgwell, A. J. & Lunt, D. J. Assessing the regional disparities in geoengineering impacts. *Geophys. Res. Lett.* **37**, (2010).
9. Ricke, K. L., Moreno-Cruz, J. B. & Caldeira, K. Strategic incentives for climate geoengineering coalitions to exclude broad participation. *Environ. Res. Lett.* **8**, 014021 (2013).
10. Crook, J., Jackson, L. S., Osprey, S. M. & Forster, P. M. A Comparison of Temperature and Precipitation Responses to Different Earth Radiation Management Geoengineering Schemes. *J. Geophys. Res. Atmospheres* **120**, 9352–9373 (2015).
11. van der Wiel, K. *et al.* The Resolution Dependence of Contiguous U.S. Precipitation Extremes in Response to CO2 Forcing. *J. Clim.* **29**, 7991–8012 (2016).
12. Kravitz, B. *et al.* The Geoengineering Model Intercomparison Project (GeoMIP). *Atmospheric Sci. Lett.* **12**, 162–167 (2011).

13. National Research Council. *Climate Intervention: Reflecting Sunlight to Cool Earth*. (National Academies Press, 2015).
14. Irvine, P. J., Kravitz, B., Lawrence, M. G. & Muri, H. An overview of the Earth system science of solar geoengineering. *Wiley Interdiscip. Rev. Clim. Change* n/a-n/a (2016). doi:10.1002/wcc.423
15. Boucher, O. *et al.* Clouds and Aerosols. in *Climate Change 2013: The Physical Science Basis. Contribution of Working Group I to the Fifth Assessment Report of the Intergovernmental Panel on Climate Change* (eds. Stocker, T. F. et al.) (Cambridge University Press, 2013).
16. MacMartin, D. G., Ricke, K. L. & Keith, D. W. Solar geoengineering as part of an overall strategy for meeting the 1.5°C Paris target. *Phil Trans R Soc A* **376**, 20160454 (2018).
17. Jones, A. C. *et al.* Regional Climate Impacts of Stabilizing Global Warming at 1.5 K Using Solar Geoengineering. *Earths Future* **6**, 230–251 (2018).
18. Robock, A., Oman, L. & Stenchikov, G. L. Regional climate responses to geoengineering with tropical and Arctic SO2 injections. *J. Geophys. Res.-Atmospheres* **113**, D16101 (2008).
19. Swann, A. L. S., Hoffman, F. M., Koven, C. D. & Randerson, J. T. Plant responses to increasing CO2 reduce estimates of climate impacts on drought severity. *Proc. Natl. Acad. Sci.* **113**, 10019–10024 (2016).
20. MacMartin, D. G., Caldeira, K. & Keith, D. W. Solar geoengineering to limit the rate of temperature change. *Philos. Trans. R. Soc. Math. Phys. Eng. Sci.* **372**, (2014).
21. Dai Z., Weisenstein D. K. & Keith D. W. Tailoring Meridional and Seasonal Radiative Forcing by Sulfate Aerosol Solar Geoengineering. *Geophys. Res. Lett.* **45**, 1030–1039 (2018).
22. Kravitz Ben *et al.* First Simulations of Designing Stratospheric Sulfate Aerosol Geoengineering to Meet Multiple Simultaneous Climate Objectives. *J. Geophys. Res. Atmospheres* **122**, 12,616-12,634 (2018).
23. Keith, D. W., Weisenstein, D. K., Dykema, J. A. & Keutsch, F. N. Stratospheric solar geoengineering without ozone loss. *Proc. Natl. Acad. Sci.* **113**, 14910–14914 (2016).

24. Murakami, H. *et al.* Simulation and Prediction of Category 4 and 5 Hurricanes in the High-Resolution GFDL HiFLOR Coupled Climate Model. *J. Clim.* **28**, 9058–9079 (2015).
25. Bhatia, K., Vecchi, G. A., Murakami, H., Underwood, S. D. & Kossin, J. Projected Response of Tropical Cyclone Intensity and Intensification in a Global Climate Model - SUBMITTED. *J. Clim.* (2018).
26. Kravitz, B. *et al.* Climate model response from the Geoengineering Model Intercomparison Project (GeoMIP). *J. Geophys. Res. Atmospheres* **118**, 8320–8332 (2013).
27. Emanuel, K. Increasing destructiveness of tropical cyclones over the past 30 years. *Nature* **436**, 686–688 (2005).
28. Curry, C. L. *et al.* A multi-model examination of climate extremes in an idealized geoengineering experiment. *J. Geophys. Res. Atmospheres* **119**, 3900–3923 (2014).
29. Jones, A. C. *et al.* Impacts of hemispheric solar geoengineering on tropical cyclone frequency. *Nat. Commun.* **8**, 1382 (2017).
30. Wang, Q., Moore, J. C. & Ji, D. A statistical examination of the effects of stratospheric sulfate geoengineering on tropical storm genesis. *Atmospheric Chem. Phys.* **18**, 9173–9188 (2018).
31. Emanuel, K., Sundararajan, R. & Williams, J. Hurricanes and Global Warming: Results from Downscaling IPCC AR4 Simulations. *Bull. Am. Meteorol. Soc.* **89**, 347–368 (2008).
32. Walsh, K. J. E. *et al.* Tropical cyclones and climate change. *Wiley Interdiscip. Rev. Clim. Change* **7**, 65–89 (2016).
33. Emanuel, K. A. Downscaling CMIP5 climate models shows increased tropical cyclone activity over the 21st century. *Proc. Natl. Acad. Sci.* **110**, 12219–12224 (2013).
34. Emanuel, K. A simple model of multiple climate regimes. *J. Geophys. Res. Atmospheres* **107**, ACL 4-1-ACL 4-10 (2002).

Methods

Models and experiments

GFDL HiFLOR

We employ the Geophysical Fluid Dynamics Lab (GFDL) HiFLOR model[1], a higher atmospheric resolution version of the GFDL FLOR model [2,3]. The atmosphere and land components of HiFLOR are taken from the Coupled Model, version 2.5 (CM2.5) [4] developed at GFDL, whereas the ocean and sea ice components are based on the GFDL Coupled Model, version 2.1 (CM2.1) [5–7]. HiFLOR employs a cubed-sphere geometry [8] with a 25-km mesh in the atmosphere and land components, and a 1° latitude-longitude tripolar mesh (with meridional refinement near the equator) for sea ice and ocean components; physical processes and the ocean component were inherited from FLOR (50-km cubed-sphere mesh for atmosphere and land) with only minor changes to the dynamical core and physical parameterizations. In increasing the dynamical core atmospheric resolution, the dynamical time step of the model was halved but the physics time step (time step of the convection, cloud, and radiation schemes in the model) was kept the same as in FLOR [1]. The full details of the setup of HiFLOR can be found in Murakami et al. [1]

HiFLOR can simulate Tropical Cyclones up to category 5, capturing their structure, spatial distribution and interannual variations, and is the first global coupled model that has been able to do this [1]. HiFLOR produces skilled seasonal forecasts of the number of intense tropical cyclones and the number of land-falling tropical cyclones that are better than the earlier FLOR model [9]. HiFLOR is better able to reproduce the observed tropical sea-surface temperature and precipitation climatology which means that it has a more realistic walker circulation and an improved simulation of the tropical cyclone response to the El Nino Southern Oscillation [10]. The higher resolution of HiFLOR (0.25°) compared to FLOR (0.5°), CM2.5 (0.5°), or CM2.1 (2.0°, a resolution typical of GeoMIP and CMIP5 models) allows for a far better simulation of all aspects of observed precipitation extremes in the US [11]. Whilst a similar mean intensification of precipitation has been found across these model resolutions, HiFLOR predicts a substantial increase in intense precipitation associated with tropical cyclones across the US Southeast that is not captured by the lower resolution model [11].

For GFDL HiFLOR a 300-yr control climate simulation was run with radiative forcing and land-use conditions representative of the year 1990 and initiated with 1990 observations [1]. The fixed forcing agents for the control simulations are atmospheric CO_2, CH_4, N_2O, halons, tropospheric and stratospheric O_3, anthropogenic tropospheric sulfates, black and organic carbon, and solar irradiance. The $2xCO_2$ experiment starts in year 100 of the control simulation with a 1% per year increase in CO_2 concentrations that halts at year 170, the point of doubling, and remains fixed until the end of the simulation in year 300. HiFLOR has an equilibrium climate sensitivity of 2.8 °C and a transient climate response of 1.53 °C. The half-SG simulation begins at year 170 of the $2xCO_2$ experiment with an instantaneous 1% reduction in solar constant and runs until year 300. This experiment is referred to as half-SG as it offsets roughly half of the warming from the $2xCO_2$ experiment (53%: $2xCO_2$ is 2.0°C warmer than control and half-SG 0.93°C warmer). The last 100 years are used for the averaging period. A single member was run for each experiment.

GeoMIP

For the GeoMIP ensemble we draw on 12 models from the GeoMIP G1 set of experiments (Extended Data Table 5.) [12]. Table 1 of Kravitz et al. [13] lists the model setups for all GeoMIP models analyzed here and provides an overview of the climate response of these models for the GeoMIP G1 experiment. The pre-industrial control experiment is specified as in the Coupled Model Intercomparison Project phase 5 (CMIP5) [14]. The 4xCO_2 experiment spins off from the pre-industrial control with an instantaneous quadrupling of CO_2 concentrations. The G1 experiment is the same as the 4xCO_2 experiment but with an instantaneous reduction in solar constant chosen to restore the global-mean top-of-atmosphere radiative balance to that of the pre-industrial in so far as possible. This experiment is referred to here as full-SG as it offsets all of the warming from the 4xCO_2 experiment. The G1 experiment runs for a total of 50 years and the last 40 years are used for the averaging period, the matching 40 years are used as the averaging period for the other two experiments. A single ensemble member is used for each model and experiment.

Downscaled Tropical Cyclone Simulations

The downscaling technique is described in detail in Emanuel et al. [15,16]. The technique begins by randomly seeding with weak hurricane-like disturbances the large-scale, time-evolving state given by the global climate data. These seed disturbances are assumed to move with the large-scale flow in which they are embedded, plus a westward and poleward component owing to planetary curvature and rotation. Their intensity is calculated using a simple, circularly symmetric hurricane model coupled to a very simple upper ocean model to account for the effects of upper ocean mixing of cold water to the surface. Applied to the synthetically generated tracks, this model predicts that a large majority of seed storms dissipate owing to unfavorable environments. Only the 'fittest' storms survive; thus the technique relies on a kind of natural selection. The model is extremely fast and many thousands or tens of thousands of storms can easily be simulated. Extensive comparisons to historical events by Emanuel et al. (2008)[16] and subsequent papers provide confidence that the statistical properties of the simulated events are consistent with those of historical tropical cyclones.

Scaling

To produce comparable results to the half-SG experiment of GFDL HiFLOR we scale the results of GeoMIP G1 to estimate the climate response of a solar constant reduction that offsets only half the radiative forcing from the 4xCO_2 experiment. The scaled results are calculated as follows:

$$X_f = X_{4\times CO_2} + f * \left(X_{G1} - X_{4\times CO_2}\right)$$

Where X is the variable to be scaled and f is the fraction of the 4xCO_2 radiative forcing offset (0.5 for half-SG). The scaling is applied not only to the means but also to the standard deviations as well for the purposes of calculating statistical significance. The same function is used to scale the results of the half-SG GFDL HiFLOR experiment to produce Extended Data Figure 5.

Previous studies of solar geoengineering have evaluated the response across a range of scenarios with different radiative forcings finding an approximately linear response to forcing magnitude at the regional level for temperature and precipitation [17,18]. However, some aspects of the response are not linear, for example Schaller et al. (2014)[19] found that the poleward energy transport did not respond linearly to combinations of solar and CO_2 forcing. To test the performance of this linearity assumption for our study, we ran simulations with CESM 1.2[20] that mirrored the GeoMIP experiments and also included an experiment which offset half the radiative forcing from the 4xCO_2

experiment. Extended Data Table 4 reproduces Table 1 for the simulated and linearly-scaled half-SG case for CESM 1.2. The results are broadly similar, but the areas reported differ by a few percent. The linearly-scaled GeoMIP half-SG results should thus provide a reasonable estimate of the half-SG response that would be simulated.

Variables

We evaluate annual-mean surface (2m) air temperature (T) and annual-mean precipitation minus evaporation (PE) for all models. We also evaluate two indices of daily extremes from the Expert Team on Climate Change Detection and Indices (ETCCDI) [21]: maximum annual surface air temperature (TXx referred to here as Tx) and maximum annual 5-day precipitation (Rx5day, referred to here as Px). These extreme indices were available for only 8 of the 12 GeoMIP models (see Extended Data Table 5). These extreme indices data were the same as used in Curry et al [22]. These extreme indices were regridded to a median model grid resolution of 144 × 96 (2.5◦ longitude × 1.9◦ latitude), which corresponds to the grid of the NorESM1-M model. A first-order conservative remapping algorithm was used [23], carried out using the Climate Data Operators package (CDO, http://code.zmaw.de/projects/cdo).

We include both T and Tx as T is a good predictor of general climate regime shifts and Tx is a good indicator for extreme heat risk. We focus on annual-mean PE as an indicator of overall changes to long-run water availability and exclude precipitation from our analysis in the main text as it does not capture the substantial changes in evapotranspiration expected due to the direct physiological effect of CO_2 on plants and the reduced surface energy availability that results from reduced insolation at the surface [24,25]. Px is a good predictor of changes in large-scale flooding events such as those accompanying Hurricane Harvey [26]. We do not address sea-level rise in this study but all indications are that solar geoengineering would reduce global sea-level rise, though its efficacy is uncertain [27,28].

We also evaluate the global-mean of the tropical cyclone Power Dissipation Index (PDI) for the HiFLOR model:

$$\mathrm{PDI} \equiv \int_0^{\tau} V_{\max}^3 \, \mathrm{d}t$$

Where V_{max} is the maximum sustained wind speed at 10 m, and the integral is over τ, the lifetime of the storm [29]. PDI gives an approximation to the total power dissipation of a tropical storm and is an indication of the total threat posed by the storm.

Together these variables cover most of the drivers of the key risks of climate change identified by the IPCC AR5 WG2. Table TS3 from this report lists the physical hazards and vulnerabilities that combine to create these key risks. Extended Data Table 1 compares the physical hazards listed in that table with the 5 variables analyzed here and shows that together they cover most of the drivers of these key hazards.

Weightings and masks

land area without Greenland and Antarctica

Bounding boxes for Greenland and Antarctica were defined and for GFDL the fraction of land within each was set to zero. The Antarctic definition included all land below 60S and the Greenland definition was defined as a polygon with corners at the following coordinates:

[[-73.5E, 78.8N], [-73.5E, 74.5N], [-44.5E, 57.5N], [-10E, 73.5N], [-10E, 84.5N], [-37.5E, 84.5N], [-60.5E, 82.5N]]

For GeoMIP, the high-resolution GFDL bounding box was regridded to each model's grid using the distance-weighted average regridding routine of CDO and used to adjust down the fraction of land within each gridcell.

Population-weighting

We employed the GPWv4 gridded population dataset to create a count of population within each model gridcell [30]. For each gridcell we summed all gridded GPWv4 population counts whose centroid was within the gridcell boundaries.

Statistical Test for Exacerbation and Moderation

We define a region as exacerbated when the half-SG anomaly has a greater absolute magnitude than the $2xCO_2$ anomaly. We test for statistical significance by first running a 90% T-Test using the absolute anomalies and the standard deviations of half-SG and $2xCO_2$. Two additional 90% T-Tests are run to determine whether $2xCO_2$ and half-SG are each statistically significantly different from the control. If the absolute anomalies are significantly different but both $2xCO_2$ and half-SG are not significantly different from the control, then we count the statistical test as failed. In the case that the absolute anomalies are significantly different but one other test is failed there are two options: i) if $2xCO_2$ is not significantly different from control and half-SG is then the region must report an exacerbation, ii) if $2xCO_2$ is significantly different from control and half-SG is not then the region must report a moderation. As our analysis focuses on changes in annual-mean climate, the sample size for the T-Test is defined as equal to the number of years in the averaging period, i.e. 100 years for HiFLOR and 40 years for the GeoMIP models. In the regional analysis the regional mean is taken before the standard deviation is calculated.

Regional analysis

We use the IPCC Special Report on Extremes (SREX) region definitions for figure 3[31]. These region definitions were used to create masks on the GFDL HiFLOR grid. These high-resolution masks were then regridded to each GeoMIP model grid using the distance-weighted average regridding routine of CDO. For each variable, the land-area mean of each regional mask was taken to produce annual-average timeseries. From these timeseries the mean and standard deviation for the evaluation period were calculated.

Data Availability

The GeoMIP and CMIP5 data used in this study is available on the Earth System Grid (https://www.earthsystemgrid.org/), the processed HiFLOR data used in this study will be made available upon request.

References

1. Murakami, H. *et al.* Simulation and Prediction of Category 4 and 5 Hurricanes in the High-Resolution GFDL HiFLOR Coupled Climate Model. *J. Clim.* **28,** 9058–9079 (2015).
2. Jia, L. *et al.* Improved Seasonal Prediction of Temperature and Precipitation over Land in a High-Resolution GFDL Climate Model. *J. Clim.* **28,** 2044–2062 (2014).
3. Vecchi, G. A. *et al.* On the Seasonal Forecasting of Regional Tropical Cyclone Activity. *J. Clim.* **27,** 7994–8016 (2014).
4. Delworth, T. L. *et al.* Simulated Climate and Climate Change in the GFDL CM2.5 High-Resolution Coupled Climate Model. *J. Clim.* **25,** 2755–2781 (2012).
5. Delworth, T. L. *et al.* GFDL's CM2 Global Coupled Climate Models. Part I: Formulation and Simulation Characteristics. *J. Clim.* **19,** 643–674 (2006).
6. Gnanadesikan, A. *et al.* GFDL's CM2 Global Coupled Climate Models. Part II: The Baseline Ocean Simulation. *J. Clim.* **19,** 675–697 (2006).
7. Wittenberg, A. T., Rosati, A., Lau, N.-C. & Ploshay, J. J. GFDL's CM2 Global Coupled Climate Models. Part III: Tropical Pacific Climate and ENSO. *J. Clim.* **19,** 698–722 (2006).
8. Putman, W. M. & Lin, S.-J. Finite-volume transport on various cubed-sphere grids. *J. Comput. Phys.* **227,** 55–78 (2007).
9. Murakami, H. *et al.* Seasonal Forecasts of Major Hurricanes and Landfalling Tropical Cyclones using a High-Resolution GFDL Coupled Climate Model. *J. Clim.* **29,** 7977–7989 (2016).
10. Zhang, W. *et al.* Improved Simulation of Tropical Cyclone Responses to ENSO in the Western North Pacific in the High-Resolution GFDL HiFLOR Coupled Climate Model. *J. Clim.* **29,** 1391–1415 (2015).
11. van der Wiel, K. *et al.* The Resolution Dependence of Contiguous U.S. Precipitation Extremes in Response to CO2 Forcing. *J. Clim.* **29,** 7991–8012 (2016).
12. Kravitz, B. *et al.* The Geoengineering Model Intercomparison Project (GeoMIP). *Atmospheric Sci. Lett.* **12,** 162–167 (2011).

13. Kravitz, B. *et al.* Climate model response from the Geoengineering Model Intercomparison Project (GeoMIP). *J. Geophys. Res. Atmospheres* **118,** 8320–8332 (2013).
14. Taylor, K. E., Stouffer, R. J. & Meehl, G. A. An Overview of CMIP5 and the Experiment Design. *Bull. Am. Meteorol. Soc.* **93,** 485–498 (2011).
15. Emanuel, K., Ravela, S., Vivant, E. & Risi, C. A Statistical Deterministic Approach to Hurricane Risk Assessment. *Bull. Am. Meteorol. Soc.* **87,** 299–314 (2006).
16. Emanuel, K., Sundararajan, R. & Williams, J. Hurricanes and Global Warming: Results from Downscaling IPCC AR4 Simulations. *Bull. Am. Meteorol. Soc.* **89,** 347–368 (2008).
17. Irvine, P. J., Ridgwell, A. J. & Lunt, D. J. Assessing the regional disparities in geoengineering impacts. *Geophys. Res. Lett.* **37,** (2010).
18. Moreno-Cruz, J. B., Ricke, K. L. & Keith, D. W. A simple model to account for regional inequalities in the effectiveness of solar radiation management. *Clim. Change* **110,** 649–668 (2012).
19. Schaller, N., Sedláček, J. & Knutti, R. The asymmetry of the climate system's response to solar forcing changes and its implications for geoengineering scenarios. *J. Geophys. Res. Atmospheres* **119,** 5171–5184 (2014).
20. Hurrell, J. W. *et al.* The community earth system model: a framework for collaborative research. *Bull. Am. Meteorol. Soc.* **94,** 1339–1360 (2013).
21. Karl, T. R., Nicholls, N. & Ghazi, A. CLIVAR/GCOS/WMO Workshop on Indices and Indicators for Climate Extremes Workshop Summary. in *Weather and Climate Extremes* 3–7 (Springer, Dordrecht, 1999). doi:10.1007/978-94-015-9265-9_2
22. Curry, C. L. *et al.* A multi-model examination of climate extremes in an idealized geoengineering experiment. *J. Geophys. Res. Atmospheres* **119,** 3900–3923 (2014).
23. Jones, P. W. First- and Second-Order Conservative Remapping Schemes for Grids in Spherical Coordinates. *Mon. Weather Rev.* **127,** 2204–2210 (1999).

24. Irvine, P. J. *et al.* Key factors governing uncertainty in the response to sunshade geoengineering from a comparison of the GeoMIP ensemble and a perturbed parameter ensemble. *J. Geophys. Res. Atmospheres* **119,** 2013JD020716 (2014).
25. Swann, A. L. S., Hoffman, F. M., Koven, C. D. & Randerson, J. T. Plant responses to increasing CO2 reduce estimates of climate impacts on drought severity. *Proc. Natl. Acad. Sci.* **113,** 10019–10024 (2016).
26. Oldenborgh, G. J. van *et al.* Attribution of extreme rainfall from Hurricane Harvey, August 2017. *Environ. Res. Lett.* **12,** 124009 (2017).
27. Irvine, P. J., Sriver, R. L. & Keller, K. Tension between reducing sea-level rise and global warming through solar-radiation management. *Nat. Clim. Change* **2,** 97–100 (2012).
28. Irvine, P. J., Keith, D. W. & Moore, J. Brief communication: Understanding solar geoengineering's potential to limit sea level rise requires attention from cryosphere experts. *Cryosphere Discuss* **2018,** 1–15 (2018).
29. Emanuel, K. Increasing destructiveness of tropical cyclones over the past 30 years. *Nature* **436,** 686–688 (2005).
30. GPWv4. Documentation for the Gridded Population of the World, Version 4 (GPWv4).
31. Seneviratne, S. I. *et al.* Appendix 3.A – Notes and technical details on Chapter 3 figures. in *Managing the Risks of Extreme Events and Disasters to Advance Climate Change Adaptation* (Intergovernmental Panel on Climate Change (IPCC), 2012).